CNWRA *A center of excellence in earth sciences and engineering*

A Division of Southwest Research Institute™
6220 Culebra Road • San Antonio, Texas, U.S.A. 78228-5166
(210) 522-5160 • Fax (210) 522-5155

October 23, 2001
Contract No. NRC–02–97–009
Account No. 20.01402.871

U.S. Nuclear Regulatory Commission
ATTN: Dr. John W. Bradbury
Division of Waste Management
Two White Flint North
Mail Stop TD–13
Washington, DC 20555

Subject: Transmittal of the deliverable "Molecular Dynamics Study of Aqueous Uranyl Interactions with Quartz (010)—Journal Paper" (IM 01402.871.200).

Dear Dr. Bradbury:

The enclosed paper is identified as IM 1402.871.200 in the fiscal year 2002 CNWRA Operations plans for the Key Technical Issue on Radionuclide Transport. The proposed title for this manuscript is "Molecular Dynamics Study of Aqueous Uranyl Interactions with Quartz (010)." The manuscript will be submitted for publication in the Journal of Physical Chemistry–B.

The U.S. Department of Energy has identified radionuclide transport in the unsaturated and saturated zones as principal factors in the postclosure performance of the proposed repository at Yucca Mountain, Nevada. Sorption is an important mechanism for retarding the movement of radionuclides from the repository horizon to the biosphere, and information is needed on the sorption of radionuclides over a wide range of geochemical conditions. Such information is used to calibrate modeling approaches employed in performance assessments of nuclear waste repositories. This manuscript describes a study of uranium sorption on the mineral quartz using molecular simulation techniques. These techniques complement information derived from batch sorption experiments conducted at the CNWRA by providing an improved mechanistic basis for evaluating experimental results. This improved technical basis will allow us to constrain our modeling and performance assessment abstractions of sorption as we further refine our understanding of the risk posed by radionuclide transport.

Washington Office • Twinbrook Metro Plaza #210
12300 Twinbrook Parkway • Rockville, Maryland 20852-1606

Publication of this manuscript serves in part to convey to the public the technical bases for U.S. Nuclear Regulatory Commission (NRC) work in the area of radionuclide sorption and transport and contributes to the NRC strategic goal of increasing public confidence.

If you have any questions regarding this submittal, please contact me 210.522.5540 or Dr. Roberto T. Pabalan 210.522.5304.

Sincerely yours,

English C. Pearcy
GHGC Element Manager

ECP: ar
enclosure

cc: J. Linehan
B. Meehan
E. Whitt
W. Reamer
K. Stablein
J. Ciocco
B. Leslie
W. Dam
W. Patrick
CNWRA Directors
CNWRA Element Managers
R. Pabalan

Molecular Dynamics Study of Aqueous Uranyl Interactions with Quartz (010)

Jeffery A. Greathouse*†, Robert J. O'Brien†, Gregory Bemis†, Roberto T. Pabalan‡

Department of Chemistry, St. Lawrence University, Canton, NY 13617, and Center for Nuclear Waste Regulatory Analysis, Southwest Research Institute, 6220 Culebra Road, San Antonio, TX 78238

Abstract: Molecular dynamics simulations were used to study the structure and dynamics of the uranyl ion and its aquo, hydroxy, and carbonato complexes in bulk water and near the hydrated quartz (010) surface. All simulations were performed in the constant (*NVT*) ensemble with three-dimensional periodic boundary conditions, and a slab technique was used to model the quartz-water interface. The uranyl coordination shell exhibits pentagonal bipyramidal symmetry, with carbonate and hydroxide ions readily replacing water molecules in the first shell. Radial distribution functions of the hydroxy and carbonato complexes are characterized by a consistent splitting in the equatorial shell, caused by the close proximity of hydroxide and carbonate oxygen atoms. Average U–O distances are 2.31-2.35 Å for hydroxide ions, 2.35-2.39 Å for carbonate ions, and 2.49-2.55 Å for water molecules. Two protonation states of the quartz surface were considered for adsorption simulations: singly protonated and partially deprotonated. Surface complexes formed only when the initial uranyl position was close to the surface, otherwise a diffuse species was observed. Outer-sphere surface complexes formed at the singly

* Address correspondence to this author at the following e-mail address: jgreathouse@stlawu.edu.
† St. Lawrence University
‡ Southwest Research Institute

protonated surface and are characterized by hydrogen bonding between a coordinating water molecule and the surface. Inner-sphere surface complexes formed at the partially deprotonated surface, with water and surface oxygen atoms equidistant to the uranium atom. In both types of surface complex, splitting of the equatorial shell of the uranyl ion was due to the presence of hydroxide or carbonate ions in the first coordination shell.

1. Introduction

Uranium is a major contaminant in soils, subsurface, or groundwaters of many sites in the U.S. due to mining and milling of uranium ores and to various processes related to production of nuclear reactor fuel and to manufacture of nuclear weapons.[1,2] Also, uranium is the predominant heavy metal content of spent nuclear fuel (>95 % UO_2). A major concern in the management and environmental restoration of contaminated sites and in the geologic disposal of spent nuclear fuel is the transport of uranium and other radionuclides to the biosphere as dissolved constituents in groundwater. Dissolved uranium is predominantly in the hexavalent (uranyl) form under oxidizing conditions and is potentially very mobile in the environment. An important mechanism for retarding radionuclide transport is sorption onto minerals encountered along water flow paths. To evaluate the potential migration of uranium from contaminated sites and from geologic repositories for nuclear wastes, information is needed on the sorption behavior of uranium over a wide range of geochemical conditions. Such information could be used to calibrate modeling approaches employed in performance assessments of nuclear waste repositories.

Numerous experimental studies of uranyl sorption on minerals and other types of sorbents have been published. [3-18] Most of these studies are batch experiments in which a known volume of uranyl solution is reacted with a known mass of solid, and the amount of uranium lost from

solution or sorbed on the solid is measured. The studies show that uranyl sorption at amphoteric surface hydroxyl sites of the sorbent is a function of pH, the type and concentration of complexing ligands, and the surface area or sorption site density of the sorbent. Uranyl sorption on cation-exchange sites of clays and zeolites also depend on the ionic strength or background electrolyte concentration due to competition between the uranyl ion and other cations present in the aqueous phase for the ion-exchange sites on the sorbent. Although sorption experiments provide useful information on the effects of solution chemistry and mineral sorbent properties on uranyl sorption behavior, these experiments study only the macroscopic aspects of the interaction of uranium with the mineral surface and give no direct information on the structure and local chemical environment of the sorbed species.

X-ray absorption spectroscopy (XAS), which includes X-ray absorption near-edge structure (XANES) and extended X-ray absorption fine structure (EXAFS) spectroscopy, is useful in directly probing the structure and oxidation state of sorbed metals. Published XAS studies show that uranyl sorbed on different sorbents, including silica, alumina, ferrihydrite, hematite, montmorillonite, vermiculite, hydrobiotite, kaolinite, and clinoptilolite, remains in the hexavalent state as the linear UO_2^{2+} moiety.[11,19-24] However, the equatorial coordination of uranyl is different under conditions that favor sorption at surface hydroxyl sites versus sorption at ion-exchange sites. EXAFS results show that the structure of uranyl in ion-exchange sites of montmorillonite, vermiculite, and hydrobiotite exhibits a uniform equatorial shell of oxygen ligands, with a coordination number of 5±1 and a $U–O_{eq}$ distance of ~2.4 Å, similar to that of the free uranyl pentaaquo species.[21,22,24] In contrast, the structure of uranyl sorbed on surface hydroxyl sites of silica, alumina, ferrihydrite, hematite, montmorillonite, vermiculite, hydrobiotite, kaolinite, and clinoptilolite shows a pronounced splitting into two equatorial shells

with $U–O_{eq}$ distances of ~2.3 and ~2.5 Å and a total coordination number ranging from 4 to 6.[11,19-23] The presence of equatorial splitting in the sorbed uranyl structure has been interpreted to be evidence of inner-sphere complexation of the uranyl ion with the mineral surface,[11,19-23] whereas the fairly symmetric equatorial shell for ion-exchanged uranyl has been interpreted as evidence for formation of an outer-sphere complex.[21,22] However, although XAFS provides information on the number of oxygen atoms coordinated to the uranium atom and on U–O interatomic distances, it does not determine directly if the coordinating oxygen atom is contributed by a solvating water, by a hydroxide or carbonate ligand, or by a surface hydroxyl group. Also, because of the low solubility of uranium, particularly at near-neutral to alkaline pH, XAFS analysis can be complicated by formation of oligomeric uranyl species or precipitation of a uranium solid when relatively high uranyl concentrations are used to enhance the X-ray signal.

Molecular simulation techniques can serve as a useful complement to sorption experiments and spectroscopic methods. The sorption behavior of specific uranyl species on different minerals can be studied directly through simulations of realistic models of molecular complexes and mineral surfaces. The complicating effects of oligomeric species formation and precipitation can be avoided by using a suitable number of molecular species in the simulation. In this study, we used molecular simulations to study the sorption of uranyl species on a quartz surface. We selected quartz as the sorbent for this study because it is a major rock-forming mineral in many geologic environments. For example, quartz makes up nearly one-third of the mass of geologic units surrounding the repository horizon at the proposed Yucca Mountain high-level nuclear waste repository.[25] Also, quartz has a relatively simple composition and experimental data are available on uranyl sorption on this mineral over wide ranges of uranium concentration, pH, and solid-mass/solution-volume ratio.[17]

2. Previous Molecular Simulation Studies

Rustad[26] performed theoretical calculations of hydration and water dissociation at mineral surfaces using an ionic model of water that allows for O–H bond dissociation.[27] A slab model was used, which is periodic in two dimensions but truncated in the vertical dimension by a hard ceiling. Such a model requires two-dimensional periodic boundary conditions (2D-PBC) and the appropriate Ewald sum[28] for proper treatment of Coulombic interactions. For molecular dynamics (MD) simulation of a mineral-solution interface with a full aqueous layer, Rustad concluded that a thorough sampling of all protonation states should not be expected.[26] This technique has been applied to the study of monolayer water adsorption near hematite[29] and MgO.[30] Three-dimensional slab models have been used to study water near MgO.[31] In such a model, a slab of finite thickness is constructed, and a gap above the surface is filled with water molecules. This supercell is repeated in the *x*-, *y*-, and *z*-dimensions, followed by MD simulation with three-dimensional periodic boundary conditions (3D-PBC) under the constraint of constant pressure or volume. Although the repeat of the oxide slab in the vertical dimension is unrealistic, the aqueous layer is made sufficiently thick so the structural and dynamical behavior of water at the midplane between adjacent slabs approaches that of the bulk solution. An additional complication of 3D-PBC slab simulations arises for supercells having a nonzero charge. Wasserman *et al.* found that the interaction energy between repeating hematite slabs varied with the thickness of the vacuum gap.[32]

Much of the molecular simulation research to date on the SiO_2-water interface has focused on changes in surface structure due to adsorbed water molecules. Molecular statics or dynamics calculations have been performed using semi-empirical forcefields,[33-38] but the computationally

intensive first-principles MD method has recently been used to investigate the vacuum-terminated (0001) surface of α-quartz.[39] Parker and co-workers[33,34] have performed static simulations to investigate the surface energies of various quartz crystal planes, including polarization effects in the form of a shell potential model[40] for oxygen atoms. The thermodynamics of water adsorption, both molecular physisorption and dissociative chemisorption, were also studied.[33] A key feature of their model is the relaxation of surface atoms in order to obtain precise surface energies for vacuum terminated surfaces and adsorption energies of gaseous water molecules.[34] Our method used in this study differs from Parker and co-workers[33,34] in that the bulk structure is used to represent the quartz (010) surface. Because our goal was to investigate aqueous uranyl adsorption on the surface, we focused our efforts not on the surface but instead on the aqueous phase in contact with the surface. While the adsorption energies obtained from our method are inaccurate due to the neglect of surface relaxation, the consistency of our method allows us to compare trends in sorption behavior among the various uranyl surface complexes. Our model of the quartz (010) surface is terminated both at the top and at the bottom with oxygen atoms to ensure that all silicon atoms are coordinated to four oxygen atoms, consistent with results from the relaxed surfaces.[33] Garofalini and co-workers have used 2D-PBC molecular dynamics to investigate water adsorption on silica surfaces.[35-38] Three-body terms were included in the potential energy calculations to effectively model changes in the silica surface upon the dissociative chemisorption of water molecules. The principal impact of water adsorption were the formation of surface silanols, and the bulk structure of silica was altered to a depth of approximately 8 Å below the surface. [37]

Theoretical studies of the uranyl ion in bulk aqueous solution have been carried out using MD simulations, although few potential parameters are available.[41-45] Wipff and co-workers

derived forcefield parameters for both bonded (angle bend, bond stretch) and nonbonded (Coulombic, van der Waals) interactions of aqueous UO_2^{2+} with several complexing ligands.[41-43] Nonbonded parameters for the uranium and oxygen atoms in UO_2^{2+} were first optimized to achieve a uranium coordination number of 7 in bulk water, consisting of two bonded axial oxygen atoms and five water molecules in the equatorial plane.[41] The partial charge of uranium was subsequently lowered to provide a better comparison of relative free energies of hydration.[42] Craw *et al.* derived intermolecular parameters for UO_2^{2+}, specifically for nitrate and sulfate complexes, based on *ab initio* calculations of gas-phase clusters.[44] The *ab initio* results showed partial charges for uranium and oxygen atoms in an isolated uranyl ion to be 2.8 *e* and –0.4 *e*, respectively, which changed slightly in the nitrate and sulfate complexes.[44] This partial charge for uranium is significantly higher than the values of 1.361 *e* (gas phase) and 1.342 *e* (liquid phase) obtained from a Mulliken population analysis of density functional theory (DFT) calculations of the $[UO_2(H_2O)_5]^{2+}$ complex.[46] An analysis of binding energies for uranyl complexes with four, five, and six water molecules in the first solvation shell indicates that the pentahydrate complex is most stable, with the average distance between uranium and water oxygen atoms 2.550 Å and 2.502 Å for the gas and liquid phases, respectively.[46]

Recent gas-phase quantum mechanical calculations (Möller-Plesset perturbation theory and DFT) on uranyl complexes containing H_2O and CO_3^{2-} have revealed that water molecules are significantly polarized in the $[UO_2(H_2O)_5]^{2+}$ complex, while carbonate ions are not polarized in the $[UO_2(CO_3)_3]^{4-}$ complex.[47] Additionally, uranyl-ligand dissociation energy curves showed that energy minima from forcefield-based calculations do not agree with the *ab initio* results, prompting the authors to conclude that forcefield-based simulations are inadequate to model uranyl complexes due to the neglect of polarization and charge transfer.[47] The effect of bulk

solvent in DFT calculations of $[UO_2(H_2O)_5]^{2+}$ has been included using a simple cavity model.[46] Alternatively, the recently developed *ab initio* MD technique includes polarization and charge transfer effects and has been used for simulating small aqueous systems.[48] However, for molecular simulations of the uranyl ion in aqueous environments or at the mineral-water interface, computational limitations must also be considered. Therefore, we choose to employ classical simulation techniques with fixed atomic charges on all aqueous and solid species. While our technique may neglect specific polarization effects which may result in slightly different geometries for uranyl complexes, it should be adequate for investigating trends in uranyl adsorption on the quartz (010) surface.

Here we present a comprehensive series of MD simulations of aqueous uranyl complexes with OH^- and CO_3^{2-} in bulk water and near the quartz (010) surface. These anions are common components in natural waters, and CO_3^{2-} is also likely to prevail in the groundwaters near the proposed nuclear waste storage facility in Yucca Mountain, Nevada.[49] Our goal was to investigate uranyl adsorption onto the quartz (010) surface, examining the effects of surface protonation and coordinating ligands on surface complexation and adsorption energy. Rather than incorporate surface relaxation, which would be computationally expensive, we have instead focused on the aqueous layer above the surface while leaving the quartz slab rigid. The salient features of surface protonation are still included since we allow motion of surface hydroxyl groups. We have used a classical potential model of the uranyl ion which has given good structural results for aqueous complexes with nitrato and phosphoryl ligands.[41] We tested these potential parameters for uranyl in aqueous complexes with OH^- and CO_3^{2-} by comparing our results with available experimental data on uranyl coordination geometry. After outlining our strategy for creating the quartz slab with singly protonated and partially deprotonated surfaces,

we discuss potential parameters and simulation strategy. We present results first for simulations in bulk water, followed by aqueous quartz slab simulations with both a singly protonated and a partially deprotonated quartz surface.

3. Computational Methods

3.1 Quartz Simulation Cell. All simulations were performed using the Open Force Field module of Cerius2 4.0 from Accelrys, Inc. (formerly Molecular Simulations, Inc.). We used the Crystal Builder module to create a 32-unit cell slab of α-quartz and the Surface Builder module to create the (010) surface. The simulation supercell was created with *x*- and *y*-dimensions of 19.68 and 21.65 Å, respectively, corresponding to four unit cells of quartz in each direction. The quartz slab was approximately 2 unit cells (ca. 8 Å) in depth and consisted of 88 Si atoms and 192 O atoms. The quartz slab was terminated on both top and bottom with a layer of oxygen atoms, to which protons were added to produce two singly protonated surfaces. This treatment is analogous to the dissociative chemisorption of water molecules onto a completely deprotonated quartz slab,[35] with a water H atom on the upper surface and water OH groups on the lower surface. The *z*-dimension of the supercell was fixed at 32.00 Å to allow room for water molecules and aqueous species (UO_2^{2+}, CO_3^{2-}, OH^-). Additionally, we wanted to examine uranyl adsorption near deprotonated surface oxygen atoms. Rather than creating a completely deprotonated surface, which would occur only at high pH,[50] we created a partially deprotonated surface by moving protons from a cluster of 6 surface hydroxyl groups to distant hydroxyl groups. The resulting slab consisted of 6 deprotonated surface oxygen atoms and 6 doubly protonated surface oxygen atoms with the same chemical formula as the singly protonated slab. In all slab simulations, partial charges of hydrogen and oxygen atoms at the bottom quartz

surface ($z \approx 0$) were adjusted to maintain electroneutrality for the entire supercell, thus avoiding an unwanted divergence in potential energy.[32]

3.2 Interatomic potentials. Potential parameters for aqueous species were based on the Consistent-Valence Forcefield (CVFF), which employs the flexible version of the Simple Point Charge (SPC) water model.[51] The flexible SPC water model has been used successfully for simulations of bulk liquid[52] and at the water-mineral interface.[53] Intramolecular motion (bond stretching and angle bending) was allowed for all aqueous species and for hydroxyl groups at the upper quartz surface. The remainder of the quartz surface was held rigid throughout the simulations. The potential energy component for nonbonded interactions consisted of Coulombic and van der Waals terms between atoms i and j at a separation of r. The potential energy term for bonded interactions consisted of angle bending and bond stretching terms. Other than the quartz slab, which was treated as a rigid body, no species contained more than three atoms bonded in a chain, hence a torsional term was not used. The values for parameters are given in Table 1.

Where applicable, atomic parameters were taken from CVFF or CVFF_aug, a nonbonded version for simulations of oxide minerals available with Cerius2. For quartz silicon and oxygen atoms, CVFF_aug values were used for the Lennard-Jones parameters, and partial charges were determined by the charge equilibration method of Rappé and Goddard.[54] For Si, we used a partial charge of 1.32 e, which is in agreement with 1.34 e obtained from an *ab initio* study of orthosilicic acid[55] and 1.2 e used by Skipper *et al.* in Monte Carlo simulations of clay hydrates.[56] Oxygen atoms at the surface were assigned a charge of –0.8 e.[56] Potential parameters for the uranyl ion were taken from Gilbaud and Wipff.[41,42] These parameters for uranyl result in a fivefold-coordination hydration shell in the equatorial plane with an average U-O_w distance of

2.5 Å,[42] in good agreement with experimental X-ray diffraction data of aqueous uranyl perchlorate.[57] In order to maintain consistency, partial charges for all hydrogen atoms were assigned the same value as SPC water (+0.41 *e*), except at the bottom quartz surface as discussed above. As a result, hydroxide oxygen was assigned a charge of –1.41 *e*, compared to the value of –0.82 *e* for SPC water, so that an overall charge of –1 *e* was maintained. Likewise, van der Waals parameters for hydroxide oxygen were assigned the same value as oxygen in SPC water. Slight modifications were made in the partial charges for the carbonate ion.

3.3 Simulation Methods. For simulations in bulk solution, we used a cubic supercell with edge length 18.2 Å containing 200 water molecules and the necessary ionic species. All hydrated slab simulations were conducted with 300 water molecules. Three-dimensional periodic boundary conditions were applied to the supercell in all simulations, resulting in either a bulk solution or macroscopic quartz-water system.

Before beginning a molecular dynamics simulation, the local water structure around the ions and the quartz surface was optimized for at least 500 steps using the Minimizer module of Cerius2. After minimization, the uranyl ion had already formed its primary coordination shell. MD simulations were performed in the constant (*NVT*) ensemble with the Nosé-Hoover thermostat.[28] Temperature was set to 300 K with a 0.1 ps relaxation time, although an average temperature of approximately 298 K was achieved in most simulations. A cutoff of 9 Å was used for short-range interactions and Coulombic interactions were treated using the three-dimensional Ewald sum[28]. Total simulation times were 100 ps with a timestep of 0.0005 ps.

Equilibration was achieved after 10–20 ps, as determined by monitoring running averages and fluctuations in the potential energy and temperature. Equilibrium average values for potential energy and temperature were obtained, and the (*x*, *y*, *z*) trajectories of water molecules

and aqueous species were plotted. Radial distribution functions (RDFs) were obtained in the usual manner[28] and were itemized according to either forcefield atom types (U–O_w) or by element type (U–O). This distinction allowed us to specify components of the U–O RDF peaks due to water oxygen atoms, surface oxygen atoms, or anion oxygen atoms. Orientation of the uranyl ion was monitored by calculating the angle ϕ between the O–U–O vector and the quartz surface normal:

$$\cos(\phi) = \frac{|U_z - O_z|}{1.8} \tag{1}$$

where U_z and O_z are the z-coordinates of the uranium atom and one oxygen atom of UO_2^{2+}, respectively, and 1.8 is the equilibrium U–O bond length (in Å). Thus, $\phi = 0°$ indicates that the ion is perpendicular to the surface, while $\phi = 90°$ indicates that the ion is parallel to the surface. Although the O–U–O angle and O–U bond lengths are dynamical quantities in the simulations, Equation 1 represents a reliable estimate of O–U–O orientation.

Water mobility was quantified by plotting the mean square displacement (MSD) of water oxygen atoms and calculating the self-diffusion coefficient, D_w, from the Einstein relation,[28,58]

$$\frac{1}{N}\sum_{i=1}^{N}\left\langle \left| r_i(t) - r_i(0) \right|^2 \right\rangle = 6D_w \tag{2}$$

where $r_i(t)$ is the position of the water oxygen atom at time t, and the summation extends over N water molecules. Water molecules did not substitute into the uranyl solvation shell during the 100-ps simulation, therefore solvating water molecules were not included in the MSD calculation. Our goal in creating such a large aqueous layer ($z \approx 22.5$ Å) above the quartz surface was to produce a region within the aqueous layer that mimics bulk water. Separate water regions were classified according to their distance from the upper quartz surface at the beginning of the MSD calculation: (i) water molecules within 0.0–7.5 Å of the surface (bottom third), (ii)

7.5 –15.0 Å (middle third), and (iii) 15.0 –22.5 Å (top third). MSD calculations for water molecules in the upper third of the supercell were unreliable due to the difference in partial charges for oxygen and hydrogen atoms at the lower quartz surface. We were chiefly interested in water structure near the upper quartz surface and in the middle, bulk-like aqueous region.

A comparison of adsorption energies for the uranyl surface complexes studied here is complicated by the fact that the net charge on the quartz surface depends on the quantity and charge of anion ligands present in the aqueous phase (Section 3.1). Instead, relative adsorption energies were determined by calculating the difference in average potential energy, $\langle E(N) \rangle$, between a simulation with N water molecules and the corresponding dehydrated system ($N = 0$). The resulting hydration energy is defined as[59,60]

$$\Delta E = \frac{\langle E(N) \rangle - \langle E(0) \rangle}{N} \tag{3}$$

In this manner energy differences due to the net surface charge are factored out, allowing a comparison of the average molar energy of water. Alternatively, an immersion energy Q_d may be calculated,[60]

$$Q_d = N\left[\Delta E(N) - E_{\text{bulk}}\right] \tag{4}$$

where E_{bulk} is the mean interaction energy of bulk SPC water (–11.4 kcal·mol^{-1}).

4. Results and Discussion

4.1 Bulk Solution. Results for simulations in bulk solution are presented in Table 2. All simulations in the bulk were carried out with 200 water molecules in a supercell with edge lengths of 18.2 Å. Separate simulations were performed for bulk water, one aqueous uranyl ion, and aqueous uranyl-hydroxide and uranyl-carbonate complexes consisting of one uranyl ion and

either one or two anion ligands. The equilibrium coordination shell for $[UO_2(H_2O)_5]^{2+}$ consisted of five water molecules in a pentagonal bipyramidal geometry, with uranyl oxygen atoms in the axial positions. In Figure 1, we see U–O and U–H RDFs averaged over the equilibrium portion of the simulation. The U–O RDF contains two peaks, one corresponding to the primary solvation shell at 2.49 Å and a second broader peak at 4.85 Å. This average U–O_w distance of 2.49 Å agrees well with the experimental value of 2.42 Å, obtained from proton NMR and X-ray diffraction experiments.[57] The single sharp U–H peak at 3.21 Å, indicates that the solvating water molecules are oriented such that their C_{2v} rotational axes are bisected by the bipyramidal plane.

For simulations of hydroxide and carbonate complexes, anion ligands (OH^- or CO_3^{2-}) were initially placed within 10 Å from the uranyl ion and quickly entered the first coordination sphere upon equilibration. Averaged U–O RDFs are shown in Figure 2a, with peak distances tabulated in Table 2. The presence of OH^- or CO_3^{2-} in the uranyl complex results in a split equatorial shell about the uranium atom, with oxygen atoms from OH^- or CO_3^{2-} occupying positions closer than water oxygen atoms. A likely explanation for this behavior is the increased negative charge assigned to the hydroxide oxygen atom (Table 1), which results in a stronger electrostatic attraction between uranium and hydroxide oxygen atoms relative to that between uranium and water oxygen atoms. For the uranyl hydroxy complexes, our U–OH distances are consistent with gas-phase *ab initio* calculations of the complex $[UO_2(H_2O)(OH)_4]^{2-}$, which gave U–OH and U–O_w distances of 2.43–2.47 Å and 2.65 Å, respectively.[61] Our equatorial U–OH distances are also in agreement with recent EXAFS experiments of UO_2^{2+} in aqueous tetramethylammonium hydroxide solution, in which the U–OH distance was measured to be 2.22 Å[62] and 2.24 Å.[61] However, the presence of four or five hydroxide ions in the uranyl coordination shell represents a

far more alkaline solution than those in our simulations. A similar splitting was observed from EXAFS spectra of uranium (VI) oxide precipitates in aqueous lithium hydroxide, with equatorial U–O peaks at 2.26 Å and 2.47 Å.[63] The second equatorial peak was most prominent at low LiOH (*aq*) concentration (0.1 M) and not assigned at higher concentrations (0.5 M – 5.0 M).[63] These results are consistent with our simulation results in Table 2. In strongly alkaline solution such as 5.0 M LiOH (*aq*), the equatorial shell should consist of only hydroxide ions,[62] so only one equatorial U–O peak would be present. At lower hydroxide concentrations, water molecules would enter the first coordination shell of UO_2^{2+}, resulting in a second equatorial peak.

Carbonate ions formed bidentate complexes with uranium, and a similar equatorial splitting was seen (Figure 2a and Table 3). Electrostatic considerations cannot be used to explain the difference in U–O distances in this case because the carbonate oxygen atoms are slightly more positive than water oxygen atoms (Table 1). We have found no experimental or *ab initio* results for the aqueous carbonate complexes studied here for comparison. However, the tricarbonato complex, $[UO_2(CO_3)_3]^{4-}$ has been studied. Recent EXAFS experiments show the U–O(carbonate) distance to be 2.42 Å for $[UO_2(CO_3)_3]^{4-}$ in the solid phase and 2.46 Å for the trimeric form, $[(UO_2)_3(CO_3)_6]^{6-}$, in aqueous solution.[64] Gas-phase calculations on $[UO_2(CO_3)_3]^{4-}$ show this length to be 2.58 Å.[47] For both the hydroxy and carbonato complexes, our simulation results show equatorial U–O distances in much better agreement with experiment than gas-phase quantum mechanical calculations, indicating that perhaps the presence of surrounding solvent molecules is key when performing calculations of aqueous uranyl complexes.

Water self-diffusion coefficients (D_w) were calculated from Equation 2 and are shown in Table 2. Water molecules in the first coordination shell of UO_2^{2+} were not included in the mean-square displacement calculations. For bulk water, our value of D_w is significantly lower than the

value of 41 x 10^{-10} $m^2 \cdot s^{-1}$ reported by Mizan *et al.* for flexible SPC water at 300 K.[52] While D_w was calculated for a 100-ps simulation in each case, Mizan *et al.* employed a maximum delay time of 19.9 ps for their mean square displacement calculations[52] compared to 45 ps used here. Additionally, our value is in the range of 10 x 10^{-10} $m^2 \cdot s^{-1}$ to 20 x 10^{-10} $m^2 \cdot s^{-1}$ reported by Fetter[65] and in better agreement with the experimental value of 23 x 10^{-10} $m^2 \cdot s^{-1}$ at 25 °C.[66] Water mobility is reduced when a uranyl complex is present in the simulation supercell, and a significant reduction in D_w was seen when the dicarbonato complex was present.

4.2 Singly Protonated Surface. Simulations performed with the singly protonated quartz (010) surface are summarized in Figure 2b and Table 3. First, we tested our model of the quartz-water interface with a simulation supercell constructed as described in Section 3 with 300 water molecules. An equilibrium snapshot of this supercell is shown in Figure 3. The z-axis in this supercell was held constant at 32.00 Å, which provides ample separation between the quartz slabs for water far from the surface to exhibit bulk-like properties. The space occupied by water corresponds to a density of approximately 0.96 $g \cdot cm^{-3}$, although this value is related to the influence of surface hydrogen atoms. The first O–O rdf peak is located at 2.79 (data not shown), which compares well with simulation results for flexible SPC water.[52] The second O–O peak at 4.67 Å is not consistent with bulk water, and we believe that disruption in long-range order in water is caused by the quartz surface. Water self-diffusion coefficients (D_w) were calculated using Equation 2 and are shown in Table 3. Water molecules within 7.5 Å of the quartz surface (bottom third) are less mobile than molecules between 7.5 Å and 15.0 Å above the surface (middle third). Although lower than that of bulk water, our calculated value of D_w for water far from the surface is comparable with the value obtained in our simulation of the bulk liquid. Therefore, we are confident that we have developed a workable, three-dimensional model of the

quartz-water interface that features distinct water regions near the surface and far from the surface.

To investigate uranyl adsorption onto the quartz (010) surface, a single uranyl ion was added to the 300-water supercell, at an initial U-surface distance of 6 Å. The introduction of the uranyl ion created a net charge of +2 *e* for the supercell. Partial charges of H and O atoms at the bottom of the quartz slab ($z \approx 0$) were adjusted to maintain electroneutrality for the entire supercell. Specifically, the lower surface hydrogen atoms were assigned a charge of +0.30 *e* while the lower surface oxygen atoms were assigned a charge of –0.7725 *e*, compared to values of +0.41 *e* and –0.80 *e* for the upper slab surface ($z \approx 10$ Å). This slight difference in charge of hydrogen and oxygen atoms offsets the additional +2 *e* charge created with the uranyl ion. The equilibrated structure (Figure 4a) indicates that the uranyl ion maintained its five-fold water solvation shell while forming an outer-sphere surface complex with quartz. As seen in Figure 4b, the uranyl O–U–O axis maintained an angle of approximately 45° to the surface normal. Hydrogen bonding between a solvating water molecule and the quartz surface served to lock in place the $[UO_2(H_2O)_5]^{2+}$ complex over the duration of this simulation. The average U–O_w distance of 2.51 Å (Table 3) indicates that the first coordination shell geometry of UO_2^{2+} is the same near the quartz surface as in bulk water.

Simulations with carbonate and hydroxide ions were performed, with the carbonate or hydroxide ions initially placed in close proximity to the uranyl ion. For the hydroxide ion, separate simulations were performed with a single UO_2^{2+} ion with one, two, or three OH^- in the aqueous layer. Results are not shown for the 3 OH^- simulation because no more than 2 OH^- ions were ever found in the equatorial shell of the uranyl ion. In all cases, the uranyl ion maintained a fivefold coordination shell, thus forming outer-sphere complexes with the singly protonated

quartz surface. As with simulations in the bulk, the presence of OH^- or CO_3^{2-} is indicated by a split in the equatorial shell (Figure 2b and Table 3). The averaged U–O distances are nearly identical to those in bulk solution, leading us to conclude that the singly protonated surface has little effect on the uranyl coordination geometry.

EXAFS data on uranyl sorbed on amorphous silica at pH 3.1 and 6.2 also revealed a split in the equatorial shell, with averaged U–O distances of 2.27 and 2.47 Å.[22] Similar EXAFS results have been reported for uranyl sorbed on silica gel at pH 3.5–4.0, with U–O peaks identified at 2.26–2.29 Å and 2.50–2.51 Å.[19,67] In each case, the split equatorial shell was attributed to the formation of a bidentate inner-sphere surface complex, with surface oxygen atoms residing in the equatorial shell. Our simulation results suggest that splitting occurs when the uranyl solvation shell consists of oxygen atoms in different chemical environments, and an inner-sphere surface complex may not be required. Laser-induced fluorescence spectroscopy has been used to detect the monohydroxy uranyl complex in aqueous solution between pH 3 and 4,[68] so the equatorial splitting for uranyl sorbed on silica surfaces[19,22] could be attributed to hydroxide ions in the first coordination shell. Additionally, similar experiments of uranyl adsorbed onto calcite suggest that hydroxide ions due from dissociated water molecules may be present in the uranyl coordination shell.[69]

Water self-diffusion coefficients (Table 3) show that the water layer far from the surface (middle third) is generally unaffected by the uranyl complexes. For water at the surface (bottom third), the D_w values are identical for all simulations except those with carbonate complexes. Despite the presence of bulkier carbonato ligands in the outer-sphere surface complexes, water molecules undergo motion on a slightly faster timescale than either the hydroxy or aquo complexes. One explanation could be a disruption in the hydrogen bonding network due to the

carbonato groups, compared to the increase in hydrogen bonding expected between nonsolvating water molecules with hydroxy groups and water molecules in the first coordination shell.

4.3 Deprotonated Surface. Results for simulations of UO_2^{2+} sorption near a partially deprotonated quartz surface are summarized in Figure 2c and Table 4. In the initial simulation of water near this surface, the O–O and O–H RDF peaks were identical to those values from the singly protonated surface. Next we introduced the uranyl ion near the partially deprotonated surface. As with the simulations involving a singly protonated surface, partial charges of O and H atoms at the bottom quartz surface were adjusted to maintain electroneutrality. Two simulations were performed in which the UO_2^{2+} ion was initially placed at a distance of 4.0 Å and 2.5 Å from the quartz surface. In both cases, the uranyl ion maintained its fivefold water solvation shell and never formed an inner-sphere surface complex. One of the solvating water molecules formed a hydrogen bond with the surface (see Figure 4a), which served to keep the uranium atom within 4 Å of the surface throughout each simulation, and an average U-Si distance of 6.3 Å. The RDF data showed an average U–O distance of 2.50 Å with 5 water O atoms occupying the first solvation shell. Water self-diffusion results for these two simulations were similar also (data not shown). Only when the uranyl ion was initially placed at a distance of 2.0 Å from the quartz surface did an inner-sphere surface complex form. As Table 4 indicates, the resulting surface complex, $[UO_2(H_2O)_4\{O\}]^{2+}$, had an average U–O distance of 2.50 Å. Here we use the notation {O} to indicate the presence of surface oxygen atoms in the equatorial shell of uranium. The availability of deprotonated surface oxygen atoms appears to be a prerequisite for the formation of inner-sphere uranyl surface complexes. However, our results indicate that such surface complexes form only when the initial U–surface distance was less than 2.0 Å. In addition, our results show only a single equatorial shell for this adsorbed species, in

contrast to the split equatorial shell suggested by EXAFS results of the uranyl ion adsorbed to silica surfaces.[19,22] Again, such a split equatorial shell is observed in our simulations only when another ligand (OH^- or CO_3^{2-}) is present in the equatorial shell of UO_2^{2+}.

With one or two hydroxide ions coordinated to the uranium atom, inner-sphere surface complexes also formed, but only when the uranyl species was placed within 2.0 Å of the surface, with no water molecules in between. Figure 5 shows an equilibrium snapshot of the $[(UO_2)(H_2O)(OH)_2\{O\}_2]$ surface complex. It is important to note that the surface oxygen atoms replaced only water oxygen atoms and never hydroxide oxygen atoms in the equatorial shell. Table 4 shows that the hydroxide oxygen atoms remained closer to the U atoms (2.33 Å or 2.35 Å) than the water oxygen atoms (2.53 Å or 2.55 Å), as in the singly protonated simulations. For the monohydroxy complex, $[(UO_2)(H_2O)_2(OH)\{O\}_2]^+$, the RDF peak at 2.55 Å can be assigned to oxygen atoms from both the surface and water molecules, while the hydroxide oxygen atoms formed the peak at 2.35 Å. For the dihydroxy complex, however, one surface oxygen atom was farther from the uranium atom (2.91 Å) than either the water or hydroxide oxygen atoms. For the inner-sphere surface complexes involving hydroxy ligands, the average U–Si distance is approximately 4 Å (Table 4), which does not agree with the values 2.77 Å and 3.08 Å proposed from fits of EXAFS data of uranyl surface complexes on silica.[22,67] However, a U–Si distance of 2.77 Å or 3.08 Å is possible only from a bidentate uranyl surface complex with bridging surface oxygen atoms.[22,67] Our model of the quartz (010) surface terminates with silanols, which results in a longer U–Si distance.

With carbonate ions in the simulation supercell, an inner-sphere surface complex formed when only one ion was coordinated to UO_2^{2+}, and only with monodentate surface coordination. Such a surface complex is shown in Figure **6**, with CO_3^{2-} oriented such that hydrogen bonding

occurs between one carbonate oxygen atom and surface protons. From Table 4, we again see the split equatorial shell, consisting of an inner peak of carbonate oxygen atoms and an outer peak of water and surface oxygen atoms. The dicarbonato complex $[UO_2(H_2O)(CO_3)_2]^{2-}$, with each carbonate ion acting as a bidentate ligand, never formed an inner-sphere surface complex but remained anchored to the surface via hydrogen bonding between the coordinating water molecule and the surface. One surface oxygen atom remained 2.91 Å from the uranium atom, but the first coordination shell consisted of four carbonate oxygen atoms and one water oxygen atom. For the dicarbonato complex, average U–O_L and U–O_w distances are similar to those for the singly protonated surface.

Self-diffusion coefficients for water near the partially deprotonated surface (Table 4) are in general larger than for water near the protonated surface. The presence of an inner-sphere surface complex increases water mobility in two ways. First, the surface complex does not protrude as far into the aqueous layer as an outer-sphere surface complex, thus creating less hindrance for the mobility of nonsolvating water molecules. Second, fewer nonsolvating water molecules are able to form hydrogen bonds with the surface due to the presence of the inner-sphere complex, thus increasing water mobility. The same trend in D_w holds for water in the middle region, presumably because the inner-sphere complexes never entered this region.

4.4. Adsorption Energies. Hydration energies calculated from Equation 3 are presented in Table 5. Values for water near the neutral slabs (–10.4 kcal·mol^{-1} and –10.6 kcal·mol^{-1}) are higher than that of bulk SPC water (–11.3 kcal mol–1),[52] indicating that water is in a constrained environment. Therefore, a comparison of the hydration energies from the uranyl simulations with the value from the water-only simulations provides insight into the relative stability of each complex. Only outer-sphere complexes were observed near the singly protonated surface, and of

those the pentaaquo complex had the lowest hydration energy. The monohydroxy complex also showed considerable stability, but the dihydroxy and both carbonato complexes had a null or destabilizing effect. For the inner-sphere complexes, only the pentaaquo complex showed a marked stability compared to the water-only simulation. With two carbonate ions in the coordination shell, uranyl ion forms only outer-sphere complexes with both surfaces, neither of which is favored energetically.

Immersion energies (Q_d) from Equation 4 were calculated relative to the hydrated slabs and are presented in Table 6. The Q_d values for water-only simulations (i.e., hydrated slab with no uranyl ion) were set to zero as a standard, which is analogous to replacing E_{bulk} in Equation 4 with ΔE for the water-only simulations (–10.4 kcal·mol^{-1} and –10.6 kcal·mol^{-1}). The pentaaquo complexes are energetically favored for both surface types. Except for the dihydroxy and monocarbonato complexes, the presence of surface oxygen atoms due to inner-sphere surface complexation resulted in higher immersion energies compared to the corresponding outer-sphere complexes. The unusual lowering of energy for the dihydroxy complex near the deprotonated surface is consistent with speciation studies, in which that complex is favored over the monohydroxy complex at higher pH.[68] Almost no energy difference was observed for the dicarbonato complex, which is outer-sphere near both surfaces. However, the higher hydration and immersion energies for $[UO_2(H_2O)(CO_3)_2]^{2-}$ suggest that this species is unlikely to form near the quartz (010) surface. Steric considerations have also been used to suggest that the dicarbonato complex is unlikely in aqueous solution.[70]

5. Conclusions

The range of possible uranyl orientations and motion relative to the quartz surface is summarized in Figure 7, which shows the trajectory of the *z*-coordinate of a uranium atom from three simulations. Near the partially deprotonated surface, the uranyl ion forms an inner-sphere complex involving one or two surface oxygen atoms. The uranium atom is fastened to the surface, as evidenced by the limited motion in the *z*-direction. Near the singly protonated surface, the uranyl ion forms an outer-sphere complex with hydrogen bonding between a coordinated water molecule and the surface (Figure 4a). As a result, the fully solvated ion hovers approximately 5 Å above the surface. Finally, a layer of nonsolvating water molecules can be interposed between a uranyl complex and the surface, resulting in a diffuse species. A diffuse uranyl complex is characterized by increased mobility relative to the surface, as shown by the greater variability of the *z*-coordinates in Figure 7. Two mechanisms exist for the formation of stable uranyl surface complexes. First, a uranyl ion coordinated by water molecules and/or anion ligands can form an outer-sphere surface complex, in which a solvating water molecule is hydrogen-bonded to a surface oxygen atom. This arrangement results in a U–Si distance of approximately 6 Å (Table 3). Second, a uranyl ion can form an inner-sphere surface complex, via either monodentate or bidentate coordination to surface oxygen atom(s). The average U–Si distance in this case is approximately 4 Å (Table 4). The combination of inner-sphere surface complexation between the uranium and surface oxygen atoms and additional hydrogen bonding between solvating oxygen atoms and surface protons results in an immobile surface complex. However, due to difficulties in adequate phase space sampling, inner-sphere surface complexes were not seen in our simulations unless the uranyl ion was initially placed less than 2.0 Å from the surface with no interposing water molecules. Additionally, hydration and

immersion energy calculations indicate that outer-sphere complexes that form at the singly protonated surface are in general more stable than inner-sphere complexes at the deprotonated surface. Although the aquo complexes have the lowest immersion energies at both surfaces, the outer-sphere monocarbonato and monohydroxy complexes are also quite stable at the singly protonated surface.

Previous X-ray spectroscopic results on uranyl coordination structure near silica surfaces have shown a split equatorial shell about the uranium atom, attributed to different U–O distances due to solvating water molecules and surface oxygen atoms resulting from inner-sphere surface complexes. We have considered uranyl ion adsorption onto the quartz (010) surface with two protonation states of a single crystal plane. Our MD results show that, when the uranyl ion is adsorbed via monodentate or bidentate coordination to surface oxygen atoms, water oxygen atoms and surface oxygen atoms are equidistant to the uranium atom. Equatorial splitting appears to be caused by the presence of other ligands in the first coordination shell of UO_2^{2+}, both in bulk aqueous solution and near the surface.

Acknowledgements

We wish to thank Keith Refson and David Smith for helpful discussions, and Omar F. Zaidan for assistance in preparing the figures. This work was funded by the U.S. Nuclear Regulatory Commission (NRC) under Contract Number NRC-02-97-009. G.B. is the recipient of a New York Science Education Program summer research fellowship. This paper does not necessarily reflect the views or regulatory position of the NRC. Cerius2 is a commercial software and only object codes are available to the senior author. Cerius2 is currently not under CNWRA configuration control.

References

1. National Research Council "Research Needs in Subsurface Science," Washington, D.C.: National Academy Press, 2000.

2. Riley, R. G., Zachara, J. M., and Wobber, F. J. "Chemical Contaminants on DOE Lands and Selection of Contaminant Mixtures for Subsurface Science Research," Washington, D.C.: U.S. Department of Energy, Office of Energy Research, 1992.

3. Allard, B.; Olofsson, U.; Torstenfelt, B. *Inorg. Chim. Acta* **1984**, *94*, 205.

4. Gupta, A. R.; Venkataramani, B. *Bull. Chem. Soc. Jpn.* **1988**, *61*, 1357.

5. Lieser, K. H.; Thybusch, B. *Fresenius Zeits. Anal. Chem.* **1988**, *332*, 351.

6. Sikalidis, C. A.; Alexiades, C.; Misaelides, P. *Toxicological and Environmental Chemistry* **1989**, *20/21* , 175.

7. Venkataramani, B.; Gupta, A. R. *Colloids and Surfaces* **1991**, *53*, 1.

8. Lieser, K. H.; Quandt-Klenk, S.; Thybusch, B. *Radiochim. Acta* **1992**, *57*, 45.

9. Zachara, J. M.; McKinley, J. P. *Aquat. Sci.* **1993**, *55*, 251.

10. Ticknor, K. V. *Radiochim. Acta* **1994**, *64*, 229.

11. Waite, T. D.; Davis, J. A.; Payne, T. E.; Waychunas, G. A.; Xu, N. *Geochim. Cosmochim. Acta* **1994**, *58*, 5465.

12. Idemitsu, K.; Obata, K.; Furuya, H.; Inagaki, Y. In *Scientific Basis for Nuclear Waste Management XVIII*; Murakami, T. and Ewing R., Eds.; Materials Research Society:

Pittsburgh, PA, 1994; p 981.

13. McKinley, J. P.; Zachara, J. M.; Smith, S. C.; Turner, G. D. *Clays Clay Miner.* **1995**, *45*, 586.

14. Michard, P.; Guibal, E.; Vincent, T.; LeCloirec, P. *Microporous Materials* **1996**, *5*, 309.

15. Turner, G. D.; Zachara, J. M.; McKinley, J. P.; Smith, S. C. *Geochim. Cosmochim. Acta* **1996**, *60*, 3399.

16. Pabalan, R. T.; Turner, D. R. *Aquatic Geochem.* **1997**, *2*, 203.

17. Pabalan R. T.; Turner, D. R.; Bertetti, F. P.; Prikryl, J. D. In *Adsorption of Metals by Geomedia*; Jenne, E., Ed.; Academic Press: San Diego, CA, 1998; p 99.

18. Prikryl, J. D.; Jain, A.; Turner, D. R.; Pabalan, R. T. *J. Contaminant Hydrology* **2001**, *47*, 241.

19. Reich, T.; Moll, H.; Denecke, G.; Geipel, G.; Bernhard, G.; Nitsche, H.; Allen, P. G.; Bucher, J. J.; Kaltsoyannis, N.; Edelstein, N. M.; Shuh. D.K. *Radiochim. Acta* **1996**, *74*, 219.

20. Thompson H. A.; Parks, G. A.; Brown, G. E. Jr. In *Adsorption of Metals by Geomedia*; Jenne, E., Ed.; Academic Press: San Diego, CA, 1998; p 349.

21. Hudson, E. A.; Terminello, L. J.; Viani, B. E.; Denecke, M.; Reich, T.; Allen, P. G.; Bucher, J. J.; Shuh, D. K.; Edelstein, N. M. *Clays Clay Miner.* **1999**, *47*, 439.

22. Sylwester, E. R.; Hudson, E. A.; Allen, P. G. *Geochim. Cosmochim. Acta* **2000**, *64*, 2431.

23. Bargar, J. R.; Reitmeyer, R.; Lenhart, J. J.; Davis, J. A. *Geochim. Cosmochim. Acta* **2000**, *64*, 2737.

24. Reeder, R. J.; Nugent, M.; Pabalan, R. T. In *Proceedings of the Tenth International Symposium on Water-Rock Interaction, Italy*; Cidu. R., Ed.; Swets & Zeitlinger: Lisse, The Netherlands, 2001; p 423.

25. Bish, D. L. and Chipera, S. J. "Revised Mineralogic Summary of Yucca Mountain, Nevada," Los Alamos National Laboratory, 1989.

26. Rustad J. R. *Molecular Modeling Theory: Applications in the Geosciences*; Mineralogical Society of America: Washington, DC, 2001; p 169.

27. Stillinger, F. H.; David, C. W. *J. Chem. Phys.* **1980**, *73*, 3384.

28. Allen, M. P.; Tildesley, D. J. *Computer Simulation of Liquids;* Clarendon Press: Oxford, 1987.

29. Rustad, J. R.; Wasserman, E.; Felmy, A. R. *Surf. Sci.* **1999**, *424*, 28.

30. Marmier, A., Hoang, P. N. M., Picaud, S., Girardet, C., and Lynden-Bell, R. M. *J. Chem. Phys.* **1998**; *109*, 3245.

31. Parker S. C.; de Leeuw, N. H.; Bourova, E.; Cooke, D. J. In *Molecular Modeling Theory: Applications in the Geosciences*; Cygan, R. T.; Kubicki, J. D., Eds.; Mineralogical Society of America: Washington, D.C., 2001; p 63.

32. Wasserman, E.; Rustad, J. R.; Felmy, A. R. *Surf. Sci.* **1999**, *424*, 1.

33. De Leeuw, N. H.; Higgins, F. M.; Parker, S. C. *J. Phys. Chem. B* **1999**, *103*, 1270.

34. Baram, P. S.; Parker, S. C. *Philos. Mag. B* **1996**, *73*, 49.

35. Garofalini, S. H. *J. Non-Cryst. Solids* **1990**, *120*, 1.

36. Litton, D. A.; Garofalini, S. H. *J. App. Phys.* **2001**, *89*, 6013.

37. Feuston, B. P.; Garofalini, S. H. *J. Chem. Phys.* **1989**, *91*.

38. Feuston, B. P.; Garofalini, S. H. *J. App. Phys.* **1990**, *64*, 4830.

39. Rignanese, G.-M.; De Vita, A.; Charlier, J.-C.; Gonze, X.; Car, R. *Phys. Rev. E* **2000**, *61*, 13250.

40. Dick, B. J.; Overhauser, A. W. *Phys. Rev.* **1959**, *112*, 90.

41. Guilbaud, P.; Wipff, G. *J. Phys. Chem.* **1993**, *97*, 5685.

42. Guilbaud, P.; Wipff, G. *J. Mol. Struct. (THEOCHEM)* **1996**, *366*, 55.

43. Hutschka, F.; Dedieu, A.; Troxler, L.; Wipff, G. *J. Phys. Chem. A* **1998**, *102*, 3773.

44. Craw, J. S.; Vinncent, M. A.; Hillier, I. H.; Wallwork, A. L. *J. Phys. Chem.* **1995**, *99*, 10181.

45. Hay, B. P.; Clement, O.; Sandrone, G.; Dixon, D. A. *Inorg. Chem.* **1998**, *37*, 5887.

46. Spencer, S.; Gagliardi, L.; Handy, N. C.; Ioannou, A. G.; Skylaris, C.-K.; Willetts, A. *J. Phys. Chem. A.* **1999**, *103*, 1831.

47. Hemmingsen, L.; Amara, P.; Ansoborlo, E.; Field, M. J. *J. Phys. Chem. A* **2000**, *104*, 4095.

48. Geissler, P. L.; Dellago, C.; Chandler, D.; Hutter, J.; Parrinello, M. *Science* **2001**, *291*, 2121.

49. Clark, D. L.; Hobart, D. E.; Neu, M. P. *Chem. Rev.* **1995**, *95*, 25.

50. Stumm, W. *Chemistry of the Solid-Water Interface;* John Wiley & Sons: New York, 1992.

51. Teleman, O.; Jönsson, B.; Engström, S. *Mol. Phys.* **1987**, *60*, 193.

52. Mizan, T. I.; Savage, P. E.; Ziff, R. M. *J. Phys. Chem.* **1994**, *98*, 13067.

53. Hartzell, C. J.; Cygan, R. T.; Nagy, K. L. *J. Phys. Chem. A* **1998**, *102*, 6722.

54. Rappé, A. K.; Goddard III, W. A. *J. Phys. Chem.* **1991**, *95*, 3358.

55. Sauer, J. *Chem. Phys. Lett.* **1983**, *97*, 275.

56. Skipper, N. T.; Chang, F.-R. C.; Sposito, G. *Clays Clay Miner.* **1995**, *43*, 285.

57. Aberg, M.; Ferri, D.; Glaser, J.; Grenthe, I. *Inorg. chem.* **1983**, *22*, 3986.

58. Chang, F.-R. C.; Skipper, N. T.; Sposito, G. *Langmuir* **1997**, *13*, 2074.

59. Adamson, A. W. *Physical Chemistry of Surfaces*, 5th ed.; Wiley: New York, 1990.

60. Smith, D. E. *Langmuir* **1998**, *14*, 5959.

61. Wahlgren, U.; Moll, H.; Grenthe, I.; Schimmelpfennig, B.; Maron, L.; Vallet, V.; Gropen, O. *J. Phys. Chem. A* **1999**, *103*, 8257.

62. Clark, D. L.; Conradson, S. D.; Donohoe, R. J.; Keogh, D. W.; Morris, D. E.; Palmer, P. D.; Rogers, R. D.; Tait, C. D. *Inorg. Chem.* **1999**, *38*, 1456.

63. Allen, P. G.; Shuh, D. K.; Bucher, J. J.; Edelstein, N. M.; Reich, T.; Denecke, M. A.; Nitsche, H. *J. Phys. IV* **1997**, *7*, 789.

64. Allen, P. G.; Bucher, J. J.; Clark, D. L.; Edelstein, N. M.; Ekberg, S. A.; Gohdes, J. W.; Hudson, E. A.; Kaltsoyannis, N.; Lukens, W. W.; Neu, M. P.; Palmer, P. D.; Reich, T.; Shuh, D. K.; Tait, C. D.; Zwick, B. D. *Inorg. Chem.* **1995**, *34*, 4797.

65. Fetter, C. W. *Contaminant Hydrogeology;* Macmillan Publishing: New York, New York, 1993.

66. Mills, R. *J. Phys. Chem.* **1973**, *77* , 685.

67. Reich, T.; Moll, H.; Arnold, T.; Denecke, M. A.; Hennig, C.; Geipel, G.; Bernhard, G.; Nitsche, H.; Allen, P. G.; Bucher, J. J.; Edelstein, N. M.; Shuh. D.K. *J. Elec. Spectros.* **1998**, *96*, 237.

68. Moulin, C.; Laszak, I.; Moulin, V.; Tondre, C. *Appl. Spectrosc.* **1998**, *52*, 528.

69. Geipel, G.; Reich, T.; Brendler, V.; Bernhard, G.; Nitsche, H. *J. Nucl. Mat.* **1997**, *248*, 408.

70. Meinrath, G. *J. Radioanal. Nuc. Chem.* **1996**, *211*, 349.

Table 1. Potential Parameters.

Atom Type Descriptions

Atom Type	Description
h*	H in water, the quartz surface, and OH^-
o*	O in water
O	O in UO_2^{2+}
U	U in UO_2^{2+}
O'	O in CO_3^{2-}
C	C in CO_3^{2-}
Oh	O in OH^-
Si	Si in quartz slab
Os	O in quartz slab

Table 1. Potential Parameters (continued).

Nonbonded: $E_{ij} = \frac{q_i q_j}{r} + \frac{A_i A_j}{r^{12}} - \frac{B_i B_j}{r^6}$ for the potential energy F (in kcal/mol), atomic charge q (in e), and radius r (in Å).

Atom Type	q	A	B
h*	+0.4100	0.000	0.000
o*	–0.8200	793.322	25.010
O	–0.2500	793.322	25.010
U	+2.5000	629.730	27.741
O'	–0.8100	522.394	22.336
C	+0.4300	1338.021	22.989
Oh	–1.4100	793.322	25.010
Si	+1.3200	19.197	0.000
Os	–0.6600	793.322	25.010

Table 1. Potential Parameters (continued).

Bond Stretching. $E_{ij} = k_1(r - r_0)$ for the potential energy E (in kcal·mol^{-1}), bond stretch force constant k_1, and equilibrium bond length r_0 (in Å).

Bond	k_1	r_0
U - O	1000.00	1.80
o* - h*	1106.00	1.00
O' - C	1312.00	1.25
Os – h*	1106.00	1.00
Oh – h*	1106.00	1.00

Angle Bending: $E_{ij} = k_2(\theta - \theta_0)^2$ for the potential energy E (in kcal·mol^{-1}), angle bend force constant k_2 (in kcal·mol^{-1}·rad^{-2}), and equilibrium angle θ_0 (in deg).

Angle	θ_0	k_2
O – U – O	180.00	300.00
h* - o* - h*	109.47	91.50
O' – C – O'	126.00	160.00

Table 2. Results for Simulations in Bulk Water. U–O and U–Si Distances (in Å) From Peaks in the Averaged RDFs for Ligand (O_L) and Water (O_w). Water Self-Diffusion Coefficients D_w (in 10^{-10} $m^2 \cdot s^{-1}$) for Nonsolvating Molecules Only.

Uranyl Complex	U-O_L	U-O_w	D_w
–	–	–	16.4[a]
$[UO_2(H_2O)_5]^{2+}$	–	2.51	17.8
$[UO_2(H_2O)_4(OH)]^{+}$	2.31	2.53	14.2
$[UO_2(H_2O)_3(OH)_2]$	2.33	2.53	16.2
$[UO_2(H_2O)_3(CO_3)]$	2.37	2.51	16.0
$[UO_2(H_2O)(CO_3)_2]^{2-}$	2.39	2.51	12.6

[a] Simulation of 200 water molecules only.

Table 3. Results for Simulations Near the Singly Protonated Quartz (010) Surface. U–O and U–Si Distances (in Å) From Peaks in the Averaged RDFs. Oxygen Atoms from Ligand (Hydroxide or Carbonate) and Water are Denoted by O_L and O_w, Respectively. Water Self-Diffusion Coefficients D_w (in 10^{-10} $m^2 \cdot s^{-1}$) for Nonsolvating Molecules Only.

Uranyl Complex	U-O_L	U-O_w	U-Si	D_w (bottom third)[a]	D_w (middle third)[b]
–	–	–	–	6.2[c]	14.3[c]
$[UO_2(H_2O)_5]^{2+}$	–	2.49	6.35	6.3	15.2
$[UO_2(H_2O)_4(OH)]^{+}$	2.31	2.53	8.13	6.3	15.2
$[UO_2(H_2O)_3(OH)_2]$	2.33	2.55	8.06	6.2	15.1
$[UO_2(H_2O)_3(CO_3)]$	2.37	2.51	8.25	9.7	15.1
$[UO_2(H_2O)(CO_3)_2]^{2-}$	2.37	2.51	8.03	7.1	16.4

[a] Calculated for water molecules between 0 and 7.5 Å from the surface.

[b] Calculated for water molecules between 7.5 and 15.0 Å from the surface.

[c] Results for 300 water molecules near the surface.

Table 4. Results for Simulations Near the Partially Deprotonated Quartz (010) Surface. U–O and U–Si Distances (in Å) From Peaks in the Averaged RDFs. Oxygen Atoms from Ligand (Hydroxide or Carbonate),Water, and Quartz Surface are Denoted by O_L, O_w, and O_S, Respectively. Water Self-Diffusion Coefficients D_w (in 10^{-10} $m^2 \cdot s^{-1}$) for Nonsolvating Molecules Only.

Uranyl Complex[a]	U-O_L	U-O_w	U-Os	U-Si	D_w (bottom third)[b]	D_w (middle third)[c]
–	–	–	–	–	9.0[d]	14.8[d]
$[UO_2(H_2O)_4\{O\}]^{2+}$	–	2.50	2.50	3.98	6.4	12.2
$[UO_2(H_2O)_2(OH)\{O\}_2]^{+}$	2.35	2.55	2.55	4.06	7.1	16.7
$[UO_2(H_2O)\ (OH)_2\{O\}_2]$	2.33	2.53	2.53, 2.91	4.46	7.1	16.1
$[UO_2(H_2O)_2(CO_3)\{O\}]$	2.35	2.49	2.49	3.79, 4.55	7.6	16.0
$[UO_2(H_2O)\ (CO_3)_2]^{2-}$	2.38	2.55	2.91	4.49	6.9	17.4

[a] Surface oxygen atoms in the uranium coordination shell are denoted by {O}. Charge contributions due to {O} were not included in determining the overall charge of the complex.

[b] Calculated for water molecules between 0 and 7.5 Å from the surface.

[c] Calculated for water molecules between 7.5 and 15.0 Å from the surface.

[d] Results for 300 water molecules near the surface.

Table 5. Hydration Energies (in kcal·mol^{-1}) for Uranyl Complexes. Uncertainties for all Energies are ± 0.5 kcal·mol^{-1}.

System	Singly Protonated Surface	Partially Deprotonated Surface
300 H_2O	–10.4	-10.6
300 H_2O, 1 UO_2^{2+}	–12.1	–11.7
300 H_2O, 1 UO_2^{2+}, 1 OH^-	–11.1	–10.7
300 H_2O, 1 UO_2^{2+}, 2 OH^-	–10.1	–10.7
300 H_2O, 1UO_2^{2+}, 1 CO_3^{2+}	–10.6	–10.8
300 H_2O, 1 UO_2^{2+}, 2 CO_3^{2+}	–10.5	–10.6

Table 6. Immersion Energies (in kcal·mol^{-1}) for Uranyl Surface Complexes.

System	Singly Protonated Surface	Partially Deprotonated Surface
300 H_2O	0	0
300 H_2O, 1 UO_2^{2+}	–508	–329
300 H_2O, 1 UO_2^{2+}, 1 OH^-	–209	–35
300 H_2O, 1 UO_2^{2+}, 2 OH^-	89	–41
300 H_2O, 1UO_2^{2+}, 1 CO_3^{2+}	–51	–77
300 H_2O, 1 UO_2^{2+}, 2 CO_3^{2+}	–26	–11

Figure Captions

Figure 1. Plots of the U–O (solid line) and U–H (dashed line) radial distribution functions from a simulation of UO_2^{2+} in a box of 200 water molecules. The peak due to axial oxygen atoms in UO_2^{2+} is not shown.

Figure 2. Plots of the U–O radial distribution functions from simulations in (a) bulk solution, (b) singly protonated quartz (010) surface, and (c) partially deprotonated quartz (010) surface. Ionic species in the aqueous layer are indicated next to each plot. Peaks are assigned in Tables 3–5. For the results with 1 UO_2^{2+} and 2 CO_3^{2-}, the dashed line represents the U–O_w distribution (O_w = water oxygen).

Figure 3. Equilibrium snapshot (x, z plane) of the supercell containing 300 water molecules and the singly protonated quartz (010) surface. The dashed line represents the supercell boundaries, and atomic designations are Si (orange), O (red), H (white).

Figure 4. Results from the simulation of UO_2^{2+} and 300 water molecules near the singly protonated quartz (010) surface. (a) Equilibrium snapshot (y, z plane) of the outer-sphere surface complex $[UO_2(H_2O)_5]^{2+}$, with atomic designations as in Figure 3 and U (blue). (b) Time evolution of the O–U–O vector orientation to the surface normal (Equation 2). A value of 90° indicates that the uranyl ion is oriented perpendicular to the surface.

Figure 5. Equilibrium snapshot (x,z plane) of the inner-sphere surface complex $[UO_2(H_2O)(OH)_2\{O\}_2]$, shown as large spheres. Nonsolvating water molecules and other quartz

atoms are shown as sticks. Atomic designations are Si (orange), O (red), U (blue), and H (white).

Figure 6. Equilibrium snapshot (x,z plane) of the inner-sphere surface complex $[UO_2(H_2O)_2(CO_3)\{O\}_2]$, shown as large spheres. Nonsolvating water molecules and other quartz atoms are shown as sticks. Atomic designations as in Figure 5 and C (gray).

Figure 7. Equilibrium trajectories (z-direction) of uranium atoms in inner-sphere, outer-sphere, and diffuse uranyl species. From bottom to top, the three uranyl complexes are $[UO_2(H_2O)(OH)_2\{O\}_2]$, $[UO_2(H_2O)_5]^{2+}$, and $[UO_2(H_2O)_3(OH)_2]$. Hydrogen atoms at the quartz surface have a z-coordinate of approximately 9.4 Å, so the uranium z-coordinates shown correspond to average distances of 1 Å, 4 Å, and 6 Å above the surface.

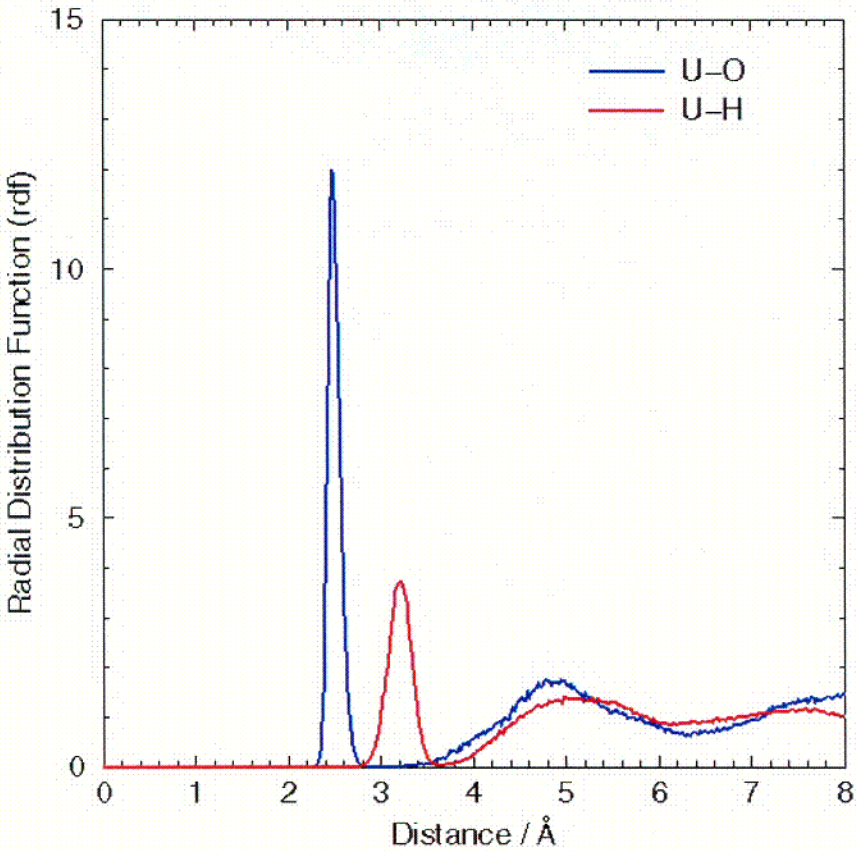
U–O
U–H
Radial Distribution Function (rdf)
Distance / Å
0
5
10
15
0
1
2
3
4
5
6
7
8

Fig 1

C01

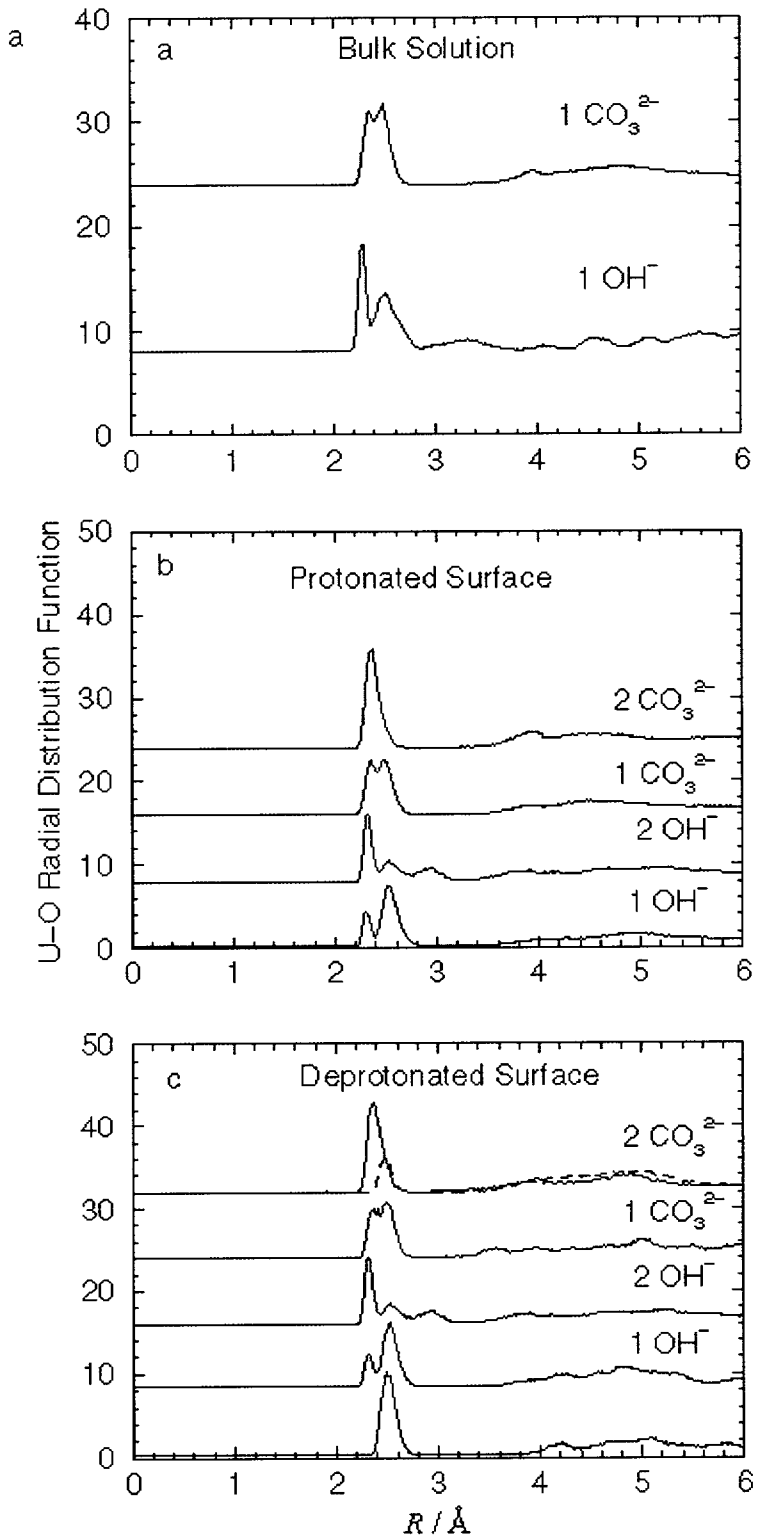
a
a
Bulk Solution
1 CO_3^{2-}
1 OH^-
b
Protonated Surface
2 CO_3^{2-}
1 CO_3^{2-}
2 OH^-
1 OH^-
c
Deprotonated Surface
2 CO_3^{2-}
1 CO_3^{2-}
2 OH^-
1 OH^-
U–O Radial Distribution Function
R / Å

Fig 2

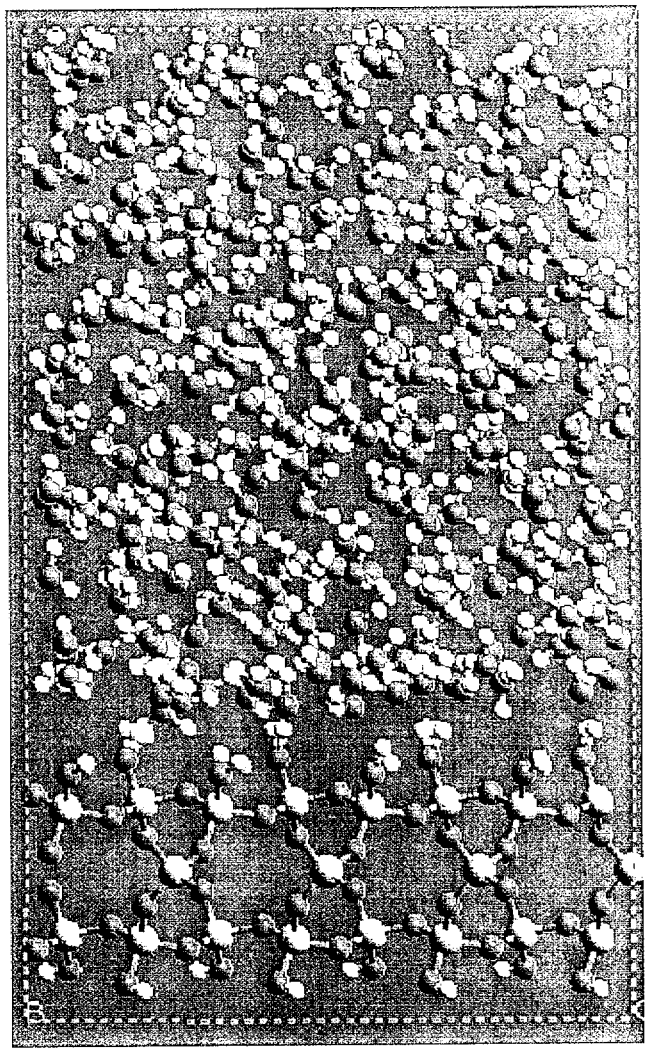

Fig 3

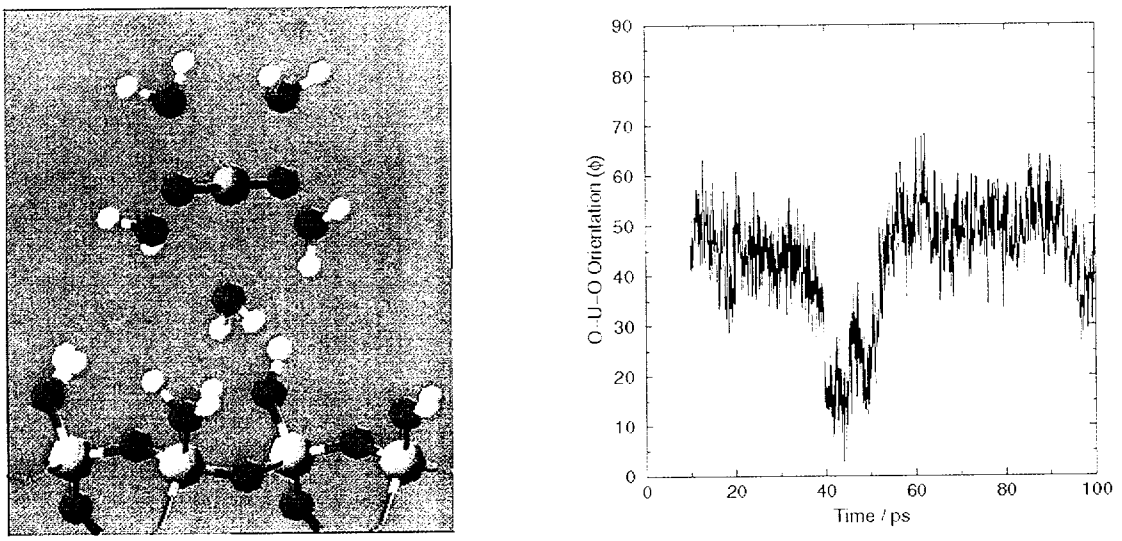
90
80
70
60
50
40
30
20
10
0
O–U–O Orientation (ϕ)
0
20
40
60
80
100
Time / ps

Fig 4

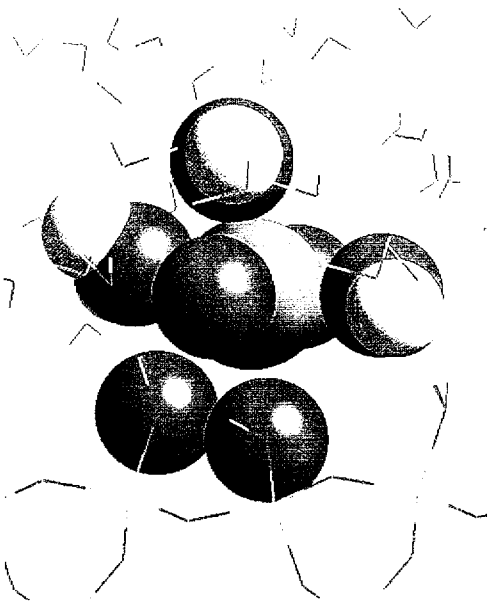

Fig 5

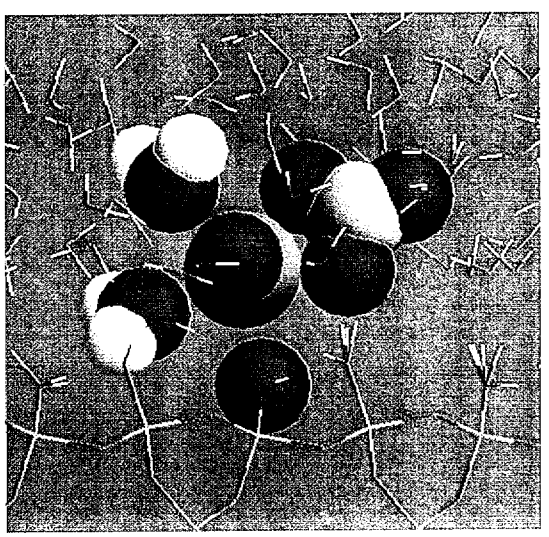

Fig 6

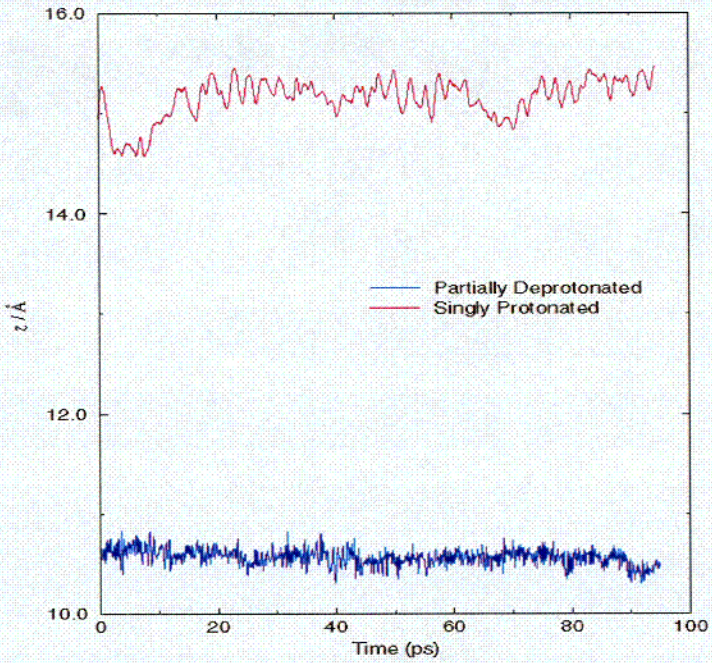
16.0
14.0
12.0
10.0
z / Å
0
20
40
60
80
100
Time (ps)
Partially Deprotonated
Singly Protonated

Fig 7

C02